Liu, X., Sun, Y., Yu, M., Yin, Y., Du, B., Tang, W., Jiang, T., Yang, B., Cao, W., & Ashfold, M. N. R. (2018). Enhanced ethanol sensing properties of ultrathin ZnO nanosheets decorated with CuO nanoparticles. *Sensors and Actuators, B: Chemical*, *255*, 3384-3390. https://doi.org/10.1016/j.snb.2017.09.165

Enhanced ethanol sensing properties of ultrathin ZnO nanosheets decorated with CuO nanoparticles

Xiao Liu[a], Ye Sun[a,*], Miao Yu[b,*], Yongqi Yin[a], Baosheng Du[a], Wei Tang[a], Tingting Jiang[b], Bin Yang[a,*], Wenwu Cao[a,c], and Michael N. R. Ashfold[d,*]

[a] *Condensed Matter Science and Technology Institute and Department of Physics, School of Science, Harbin Institute of Technology, Harbin 150080, China.*

[b] *State Key Laboratory of Urban Water Resource and Environment, School of Chemistry and Chemical Engineering, Harbin Institute of Technology, Harbin 150001, China.*

[c] *Materials Research Institute, The Pennsylvania State University, University Park, Pennsylvania 16802, U.S.A.*

[d] *School of Chemistry, University of Bristol, Bristol BS8 1TS, U.K.*

Abstract

Ultrathin two-dimensional ZnO nanosheets (NSs) with thicknesses of just a few nanometers have been fabricated by a solvothermal method. The very large surface area to volume ratio of this material translates into outstanding electrical sensing responses to ethanol (as high as S ~97 to 200 ppm of ethanol at a working temperature of 320°C). Decorating these ZnO NSs with CuO nanoparticles (NPs), by pulsed laser ablation of a CuO target at room temperature and then post-annealing at 400°C, yields CuO-ZnO NSs that display a further up to 2-fold enhanced response to ethanol vapour, reduced sensor response and recovery times, high sensing repeatability and high selectivity. Mechanisms underpinning the enhanced sensing properties of the CuO-ZnO NSs are discussed in terms of CuO NP-induced *p-n* junction depletion regions and increases in the density of active sites for ethanol adsorption and for reaction with adsorbed oxygen species.

Keywords: Zinc oxide; Copper oxide; Nanosheet; Gas sensing; *p-n* junction.

*Corresponding author. E-mail address: sunye@hit.edu.cn (Y. Sun), miaoyu_che@hit.edu.cn (M. Yu), binyang@hit.edu.cn (B. Yang), mike.ashfold@bristol.ac.uk (M.N.R. Ashfold).

1. Introduction

The enormous market demands for gas sensors in labour safety, environmental protection, medical treatment and related areas have stimulated huge interest in the development of high performance sensing materials. ZnO nanomaterials are among the most popular electrical and optical gas sensing materials, and continue to attract much attention as a result of their well-demonstrated high sensitivity (reflecting their large surface area, surface activity, and excellent electrical and luminescence properties), coupled with their low cost and simple and controllable fabrication [1–6]. A range of strategies have been applied to ZnO and ZnO-based nanomaterials in an effort to enhance the gas sensing response (sensitivity), selectivity and repeatability, and to reduce the response and recovery times, including morphology control, doping, surface modification and decoration [7–12]. Of particular relevance to the present work, CuO decoration has been shown to substantially improve the gas sensing properties of pure ZnO nanomaterials, as exemplified by studies using CuO-ZnO nanorods [13,14], nanocorals [15], composite nanowires [16], ZnO nanostructured composites [17] and hierarchical nanostructures [18]. However, the typical size of these ZnO nanostructures is of the order of a 100 nm or more, and their comparatively small surface area to volume (*S*/*V*) ratio must limit their sensing properties.

Two-dimensional (2-D) ZnO nanosheets (NSs) have shown much promise in gas sensing applications, with a range of successfully-fabricated products reported, e.g. pure ZnO NSs [19–21], Fe-doped ZnO NSs [22], Ag nanoparticle (NP)-decorated ZnO NSs [23], Pd NP-decorated NSs [24], Au-functionalized ZnO NSs [25], NiO-modified ZnO NSs [26], graphene oxide/ZnO NS nanocomposites [27], etc. The thickness of the ZnO NSs in these prior studies is typically 10–50 nm or even larger, however. Since a large *S*/*V* ratio is likely to be one of the key factors determining the sensing performance, there is obvious interest in exploring the extent to which the use of ultrathin ZnO NSs (with much reduced thickness and higher *S*/*V* ratios) can further enhance the gas sensing capability.

Here we report the design and fabrication of ultrathin 2-D ZnO NSs, their subsequent decoration with CuO NPs, and demonstrate the sensing properties of both materials to a number of different gases, including ethanol, towards which both the pristine ZnO NS samples and the CuO-ZnO NS samples show a high sensing response. Decoration with CuO NPs is shown to boost the

sensing response by as much as a factor of 2 (relative to that of the pristine ZnO NSs), and to reduce the response and recovery times. The underlying sensing mechanisms are discussed accordingly.

2. Experimental

2.1 Sample preparation

The following chemicals were used in preparing the ZnO NSs: polyethylene oxide-polypropylene oxide-polyethylene oxide (PEO_{20}-PPO_{70}-PEO_{20}, Pluronic P123, Sigma-Aldrich), ethylene glycol (EG, 98%, Sigma-Aldrich), $ZnAc_2{\cdot}2H_2O$ (99%, Aladdin), hexamethylenetetramine (HMTA, 99%, Aladdin), and ethanol (99.5%, Aladdin).

The ZnO NSs were synthesized by a facile solvothermal method reported previously [28]. Briefly, Pluronic P123 (0.4 g) was added to a mixture of ethanol (6.0 g) and H_2O (0.9 g) to form a transparent solution upon magnetic stirring for 15 min, followed by the addition of $ZnAc_2{\cdot}2H_2O$ (0.20 g) and HMTA (0.09 g). After stirring for another 15 min, 92.0 mL EG was added to the solution under stirring for 30 min. Following a static 7-day ageing process at room temperature (RT), the solution was divided equally and transferred into two 100 mL autoclaves. The sealed autoclaves were maintained at 110°C for 15 h, and the solutions then allowed to cool to RT. The ZnO NSs were obtained via three centrifugation/washing (with distilled water and ethanol) cycles. For the subsequent gas sensing measurements, or for decorating with CuO NPs, an aqueous slurry containing the ZnO NSs was pasted on commercial Ag-Pd interdigitated electrodes (Elite Tech) and then dried in a vacuum oven at RT.

CuO NP decoration of the ZnO NSs was achieved by pulsed laser ablation of a CuO ceramic target (99.99%, KAI-STAR Electo-Optic Material). Briefly, a KrF excimer laser (Lambda-Physik COMPex 205, λ = 248 nm, pulse duration = 25 ns, repetition rate = 5 Hz, and energy = 20 mJ $pulse^{-1}$) was focused onto the surface of a rotating CuO target with an illuminated area of ~1.3 mm^2 and incident fluence, F ~1.5 J cm^{-2}. The deposition was performed with a target-substrate distance d ~40 mm in a low background pressure of oxygen (p ~20 Pa) at RT. To ensure formation of CuO NPs, as well as to improve their gas sensing stability and recoverability, a post-annealing treatment in air at 400°C for 1 h was applied to

all samples (i.e. both the pristine and CuO NP decorated ZnO NS samples) before gas sensing measurements.

2.2 Characterization

The obtained samples were characterized by field emission scanning electron microscopy (FESEM, FEI, Quanta 200F), high-resolution transmission electron microscopy (HRTEM, FEI, Tecnai-G2-F30), atomic force microscopy (AFM, Asylum research, Cypher ES), X-ray diffraction (XRD, PANalytical, X'Pert Pro, with Cu Kα radiation), X-ray photoelectron spectroscopy (XPS,ESCALAB,250Xi), and spectrofluorometry (Horiba, Fluoromax-4, 325 nm excitation).

2.3 Gas sensing measurement

The sensing properties of the samples to ethanol and six other gases: methanol, ammonia, benzene, toluene, cyclohexane and tetrahydrofuran) were measured at a working temperature (T_w) of 320°C using a commercially-available intelligent gas-sensing analysis system (Elite Tech, CGS-1TP) with an 18 L test chamber [29]. In all cases, the target gas was introduced into the chamber by injecting the appropriate liquid into a heated (~200°C) quartz evaporating dish located inside the test chamber. The liquid evaporated immediately after injection and two fans in the test chamber ensured rapid and homogeneous mixing of the resulting vapor with air. After the resistance of the sensor reached an equilibrium value, the test chamber was opened and the sensor exposed to fresh air. The sensing response of the gas sensor is defined as $S = R_a / R_g$, where R_a and R_g are the resistance of the sensor in air and in the target gas, respectively. Two other important sensor characteristics are the response (t_{res}) and recovery (t_{rec}) times, which are here defined as the times required for the sensor resistance to change from, respectively, R_a to $R_a - 0.9(R_a - R_g)$ and from R_g to $R_g + 0.9(R_a - R_g)$.

3. Results and Discussion

3.1. Structure and morphology analysis

SEM and TEM analysis confirmed the typical 2-D nanosheet morphology of the pristine NS sample, and suggested NS thicknesses < 10 nm (Fig. 1a and 1b). To characterize the nanosheet thickness

more quantitatively, AFM measurements were performed using a sample prepared by dropping the pristine ZnO solution on a bare Si wafer and drying in air. The statistical results revealed an average thickness of ~4 nm, as illustrated by the example shown in Fig. 1c – which also directly demonstrates the nanosheet morphology. XRD patterns were collected also, to examine the crystallinity of the sample (Fig. 1d). All diffraction peaks can be indexed to the wurtzite crystal structure of ZnO (JCPDS 89-0510), corresponding to (100), (002), (101), (102), (110), (103), (112) and (201) planes, respectively. The crystallinity of the NSs was further confirmed by the HRTEM image (inset to Fig. 1b), which reveals parallel crystal planes with a measured spacing of ~0.26 nm, characteristic of (002) plane of ZnO.

The photoluminescence (PL) spectrum of the ZnO NS sample, recorded under 325 nm excitation (Fig. A.1), shows a narrow emission peak centered at 376 nm and a broad peak centered at 550 nm. These are assigned to ZnO near-band-gap emission and to defect / impurity-related emissions, respectively. The small blue shift of the UV emission compared to that seen in the PL spectra of many other ZnO nanomaterials [5,30–33] (which typically peaks in the 380–390 nm range) implies a significant quantum confinement effect induced by the ultrathin (few nanometer) thickness of these NSs.

As described in the Experimental section, ZnO NSs loaded on Ag-Pd electrodes were decorated with CuO NPs by pulsed laser deposition (PLD), i.e. by ablating a CuO target at RT, and then annealing in air. The amount of deposited CuO could be tuned simply by controlling the deposition time. The TEM image of the sample treated by PLD for 12 min (denoted as '*12-min CuO-ZnO*'), shown in Fig. 2a, confirms partial coverage of the ZnO NSs by additional NPs. Further HRTEM characterization (Fig. 2b) reveals that the NPs are several nanometers in dimension, and exhibit a 0.25 nm lattice spacing – characteristic of monoclinic CuO (002). Survey XPS analysis of the CuO NP decorated ZnO NS sample (Fig. 2c) reveals peaks attributable to Zn, Cu and O only (along with a C signal from exposure to the ambient environment). The high resolution XPS spectrum of the Cu2p region (Fig. 2d) shows four peaks. Those appearing at 933.6 and 953.6 eV are assigned to $Cu2p_{3/2}$ and $Cu2p_{1/2}$, respectively, while the 941.6 and 962.2 eV features are the documented shake-up satellite peaks. High resolution XPS spectra for the Zn2p and O1s regions for the '*12-min CuO-ZnO*' NS sample are shown in Fig. A.2. The XPS data demonstrate that the Cu in the sample is in the +2 oxidation state [13,34,35], and the HRTEM and XPS results both serve to confirm successful

decoration of the ZnO NSs with CuO NPs.

3.2. Gas sensing performance

As we now show, the ultrathin pristine ZnO NSs and the CuO-ZnO NSs both show particularly high sensing responses to ethanol vapor and, from here on, we largely focus on studies using ethanol as the target gas. The standard test involved measuring the time-varying resistance of each sample on the interdigitated electrode, at a working temperature T_w = 320ºC, as a function of ethanol concentration. Fig. 3 shows the time-dependent resistance measured for the pristine ZnO NS, *'2-min CuO-ZnO'* NS, *'6-min CuO-ZnO'* NS and *'12-min CuO-ZnO'* NS samples upon exposure to 20 ppm ethanol in air. The pristine ZnO NS sample shows an impressive performance, with a sensing response S ~7, and response and recovery times of, respectively, t_{res} ~6 s and t_{rec} ~36 s. Decorating the ZnO NS sample with CuO NPs leads to an increase in resistance and enhanced sensing performance; the S values determined upon exposing the *'2-min CuO-ZnO'*, '*6-min CuO-ZnO*' and '*12-min CuO-ZnO*' NS samples to 20 ppm ethanol were, respectively, ~9, 11 and 10. In addition, t_{res} and t_{rec} were both observed to decrease, to ~5 s and 25 s, respectively, for all three CuO-ZnO NS samples.

To investigate the gas sensing properties further, the dynamic response of the pristine ZnO and CuO-ZnO samples upon exposure to ethanol was measured at various T_w. Initial studies involving the pristine ZnO NS and '*6-min CuO-ZnO*' NS samples and 20 ppm of ethanol showed S increasing steadily once T_w ~200ºC and maximizing at T_w = 320ºC (Fig. A.3). As Fig. 4 shows, the sensing response of all four samples upon exposure to 1–2000 ppm ethanol at T_w = 320ºC increases with ethanol concentration, and shows high recoverability. The sensing response of the pristine ZnO NS sample at T_w = 320ºC was measured as S ~97 (to 200 ppm ethanol) rising to S ~300 at 2000 ppm ethanol. These are among the best ethanol sensing performances yet reported for any pure ZnO nanomaterial at a working temperature $T_w \leq 350$ºC (see Table A.1) [6–8,14,36–38]. Excitingly, as noted above, decorating the ZnO NSs with CuO NPs leads to further significant enhancements in the sensing response. As Fig. 4 also shows, the gas sensing properties of the '*2-min CuO-ZnO*' and '*12-min CuO-ZnO*' NS samples were quite similar over a wide range of ethanol concentrations. The '*6-min CuO-ZnO*' NS sample exhibited the highest sensing response, *e.g.* S ~130 to 200 ppm and S ~610 when exposed to 2000 ppm ethanol at T_w = 320ºC. Figure 5 highlights further favorable attributes of these sensors, including the repeatability of the response (Fig. 5a) and the high

selectivity to ethanol (and methanol, for which we measure S ~57 with the '*6- min CuO-ZnO*' NS sample when exposed to 200 ppm), *cf.* a range of other gases (ammonia, benzene, toluene, cyclohexane and tetrahydrofuran (Fig. 5b)). These data all serve to illustrate the potential of CuO-ZnO NSs in gas sensing applications.

3.3. Gas-sensing mechanism

Gas sensing mechanisms of metal oxides have been studied extensively [8−14,39−41]. Scheme 1 illustrates a plausible mechanism for the outstanding gas sensing capabilities of the ultrathin ZnO NS and CuO-ZnO NS samples. For bare ZnO nanomaterials, several groups have suggested that the formation of adsorbed oxygen species like O_2^-, O^- and O^{2-} leads to an electron depletion layer at the ZnO surface [6,7,20,24,25,27]. The reaction of ethanol (or other alcohols) with such adsorbed oxygen species will then release the trapped electrons back to the ZnO [20,32,37]. On this basis, ethanol sensing can be realized by monitoring the change of the electrical conductivity of ZnO. O^- and O^{2-} ions are the dominant adsorbed oxygen species on a ZnO surface at temperatures ~300°C [23,27,42], so the electrical sensing of ethanol by ZnO NS samples at T_W = 320°C can be expressed by the following reactions:

$$C_2H_5OH + 6O^-(ad) \rightarrow 2CO_2 + 3H_2O + 6e^- \quad (1)$$

$$C_2H_5OH + 6O^{2-}(ad) \rightarrow 2CO_2 + 3H_2O + 12e^- \quad (2)$$

The response of a metal oxide semiconductor gas sensor to changes in gas concentration is widely described using an empirical formula of the form:

$$S = \alpha C^{\beta} + 1 \quad (3)$$

or

$$\log (S - 1) = \beta \log (C) + \log \alpha, \quad (4)$$

where α is a prefactor, β is the response order that depends on the charge state of the reactive surface species, and C is the concentration of the target gas [21,22]. The value of β is ~0.5 or ~1 when the dominant reactive oxygen species is, respectively, O^{2-} and O^- [9].

The responses of the pristine ZnO, '*2-min CuO-ZnO*', '*6-min CuO-ZnO*', and '*12-min CuO-ZnO*' NS samples to changes in ethanol concentration at T_w = 320°C are all quite similar (Fig. A.4a).

Consider the '*6-min CuO-ZnO*' sample, for example. The log ($S - 1$) *vs* log (C) plot shows two distinct linear regions, characterized by slopes of, respectively, $\beta = 0.99$ at low C ($C < 20$ ppm) and $\beta = 0.69$ across the range $50 \leq C \leq 2000$ ppm (Fig. A.4b). Surface O^- species are reported to be more reactive than O^{2-} [43]. On that basis, the obtained β values can be rationally explained by assuming that O^- surface species dominate the reaction with ethanol at the lowest C (β ~1) and that O^{2-} species also play an important role in the reactions with ethanol once $C > 50$ ppm. That the pristine ZnO and the CuO-ZnO samples display similar response dependences to changes in ethanol concentration implies that CuO NP decoration (at least as implemented in the present work) does not substantially change the nature of the reactive surface oxygen species.

The large *S*/*V* ratios of the ultrathin ZnO NS samples reported in this study result in more surface sites for ethanol adsorption, thereby explaining the good sensing characteristics. The PL intensity from the ZnO NSs is reduced (~2-fold) after 6-min decoration with CuO NPs, but neither the UV near band edge feature nor the defect/impurity-related visible emission shows any discernible spectra shift upon CuO decoration (Fig. A.1), suggesting that the O-related surface defects of the ZnO NSs are barely altered by the presence of the CuO. The further boost in sensing response achieved by decorating the ZnO NSs with CuO NPs can be attributed to two factors: (i) The increase in the number of active sites for ethanol adsorption and subsequent chemical reactions that results from accommodating CuO NPs on a flat ZnO NS. We also note previous suggestions [13,17] that a CuO-decorated ZnO sample supports more active sites and more chemisorbed oxygen species than pristine ZnO which, if correct, could further facilitate ethanol adsorption and the related chemical reactions. The present finding that the '*6-min CuO-ZnO*' NS sample affords the best sensing performance would be consistent with a model where the '*2-min CuO-ZnO*' NS sample is (relatively) deficient in CuO NPs, whereas the '*12-min CuO-ZnO*' NS sample is overloaded and the extent of the CuO over-coating has depressed the sensing performance of the ZnO NS sample. (ii) The introduction of *p*-*n* junction depletion regions [10,13–18,44]. Since pure ZnO and CuO are typical *n*- and *p*-type semiconductors, respectively, the presence of the CuO NPs will give rise to localized *p*-*n* junction depletion regions within the samples. Release of electrons by reactions (1) and (2) to the ZnO and/or CuO domains would reduce these depletion regions and enhance the sensing response.

We end by highlighting the good linear relationship between log (S – 1) and log (C) at ethanol concentrations C < 20 ppm and, by implication, note that the detection limit for ethanol with both the pristine ZnO and the *CuO-ZnO* samples could extend to the ppb-level. The present work clearly represents another step along the way to optimizing the gas sensing properties of ultrathin ZnO NSs by controlled surface decoration.

4. Conclusions

Ultrathin ZnO NSs with thicknesses of just a few nanometers were fabricated by a hydrothermal method and then decorated with CuO NPs. The pristine ZnO NSs showed a high ethanol sensing response (S ~97 and ~300 to 200 ppm and 2000 ppm ethanol, respectively, at a working temperature T_w = 320°C). Decorating these ZnO NSs with CuO leads to further improvements in performance, with a significantly enhanced sensing response and reduced response and recovery times. By way of illustration, the optimized '*6-min CuO-ZnO*' NSs exhibited sensing responses as high as S ~130 and ~610 to 200 ppm and 2000 ppm ethanol, at the same T_w (320°C). These sensors also display high sensing selectivity to ethanol (a representative alcohol) and a very good repeatability of response. The impressive sensing characteristics are attributed to the very large surface area to volume ratio of the ultrathin ZnO NS base material, that are further boosted in the case of the CuO-ZnO NSs by the introduction of *p-n* junction depletion regions and an increase in the density of active sites for ethanol adsorption and reaction upon decoration with the CuO NPs.

Acknowledgements

This work was supported by the National Basic Research Program of China (973 Program) [grant number 2013CB632900]; the National Natural Science Foundation of China [grant numbers 21473045, 51401066]; the Fundamental Research Funds from the Central University [grant number PIRS OF HIT A201503].

Appendix A. Supplementary data

Supplementary data associated with this article can be found, in the online version, at http://dx.doi.org/10.1016/j.snb.XXXXXX.

References

[1] M. J. S. Spencer, Gas sensing applications of 1D-nanostructured zinc oxide: Insights from density functional theory calculations, Prog. Mater. Sci. 57 (2012) 437–486.

[2] K. Hagedorn, W. Li, Q. Liang, S. Dilger, M. Noebels, M. R. Wagner, J. S. Reparaz, A. Dollinger, J. S. A. D. Günne, T. Dekorsy, L. S. Mende, S. Polarz, Catalytically doped semiconductors for chemical gas sensing: aerogel-like aluminum-containing zinc oxide materials prepared in the gas phase, Adv. Funct. Mater. 26 (2016) 3424–3437.

[3] R. Zhou, G. Hu, R. Yu, C. Pan, Z. L. Wang, Piezotronic effect enhanced detection of flammable/toxic gases by ZnO micro/nanowire sensors, Nano Energy 12 (2015) 588–596.

[4] S. R. Ryu, S. D. G. Ram, H. D. Cho, D. J. Lee, T. W. Kang, Y. Woo, Single ZnO nanocactus gas sensor formed by etching of ZnO nanorod, Nanoscale 7 (2015) 11115–11122.

[5] X. Liu, Y. Sun, M. Yu, Y. Yin, B. Yang, W. Cao, M. N. R. Ashfold, Incident fluence dependent morphologies, photoluminescence and optical oxygen sensing properties of ZnO nanorods grown by pulsed laser deposition, J. Mater. Chem. C 3 (2015) 2557–2562.

[6] L. Wang, Y. Kang, X. Liu, S. Zhang, W. Huang, S. Wang, ZnO nanorod gas sensor for ethanol detection, Sens. Actuators B 162 (2012) 237–243.

[7] X. Luo, Z. Lou, L. Wang, X. Zheng, T. Zhang, Fabrication of flower-like ZnO nanosheet and nanorod-assembled hierarchical structures and their enhanced performance in gas sensors, New J. Chem. 38 (2014) 84–89.

[8] J. Xu, Z. Xue, Nan Qin, Z. Cheng, Q. Xiang, The crystal facet-dependent gas sensing properties of ZnO nanosheets: Experimental and computational study, Sens. Actuators B 242 (2017) 148–157.

[9] Z. Wang, Z. Tian, D. Han, F. Gu, Highly sensitive and selective ethanol sensor fabricated with In-doped 3DOM ZnO, ACS Appl. Mater. Interfaces 8 (2016) 5466–5474.

[10] X. Liu, B. Du, Y. Sun, M. Yu, Y. Yin, W. Tang, C. Chen, L. Sun, B. Yang, W. Cao, M. N. R. Ashfold, Sensitive room temperature photoluminescence-based sensing of H_2S with novel CuO−ZnO nanorods, ACS Appl. Mater. Interfaces 8 (2016) 16379–16385.

[11] M. Kumar, V. S. Bhati, S. Ranwa, J. Singh, M. Kumar, Pd/ZnO nanorods based sensor for highly selective detection of extremely low concentration hydrogen, Sci. Rep. 7 (2017) 236.

[12] S. Wang, Z. Li, P. Wang, C. Xiao, R. Zhao, B. Xiao, T. Yang, M. Zhang, Facile synthesis and enhanced gas sensing properties of In_2O_3 nanoparticle-decorated ZnO hierarchical architectures, CrystEngComm 16 (2014) 5716–5723.

[13] P. Rai, S. H. Jeon, C. H. Lee, J. H. Lee, Y. T. Yu, Functionalization of ZnO nanorods by CuO nanospikes for gas sensor applications, RSC Adv. 4 (2014) 23604–23609.

[14] Y.-B. Zhang, J. Yin, L. Li, L.-X. Zhang, L.-J. Bie, Enhanced ethanol gas-sensing properties of flower-like *p*-CuO/*n*-ZnO heterojunction nanorods, Sens. Actuators B 202 (2014) 500–507.

[15] A. Zainelabdin, G. Amin, S. Zaman, O. Nur, J. Lu, L. Hultman, M. Willander, CuO/ZnO nanocorals synthesis via hydrothermal technique: growth mechanism and their application as Humidity Sensor, J. Mater. Chem. 22 (2012) 11583–11590.

[16] J. X. Wang, X. W. Sun, Y. Yang, K. K. A. Kyaw, X. Y. Huang, J. Z. Yin, H. V. Demir, Free-standing ZnO–CuO composite nanowire array films and their gas sensing properties, Nanotechnology 22 (2011) 325704.

[17] Y. Chen, Z. Shen, Q. Jia, J. Zhao, Z. Zhao, H. Ji, A CuO–ZnO nanostructured *p*–*n* junction sensor for enhanced N-butanol detection, RSC Adv. 6 (2016) 2504–2511.

[18] N. M. Vuong, N. D. Chinh, B. T. Huy, Y. I. Lee, CuO-decorated ZnO hierarchical nanostructures as efficient and established sensing materials for H_2S gas sensors, Sci. Rep. 6 (2016) 26736.

[19] E. Modaresinezhad, S. Darbari, Realization of a room-temperature/self-powered humidity sensor, based on ZnO nanosheets, Sens. Actuators B 237 (2016) 358–366.

[20] D. Ju, H. Xu, J. Zhang, J. Guo, B. Cao, Direct hydrothermal growth of ZnO nanosheets on electrode for ethanol sensing, Sens. Actuators B 201 (2014) 444–451.

[21] L. Zhang, J. Zhao, H. Lu, L. Li, J. Zheng, H. Li, Z. Zhu, Facile synthesis and ultrahigh ethanol response of hierarchically porous ZnO nanosheets, Sens. Actuators B 161 (2012) 209–215.

[22] A. Yu, J. Qian, H. Pan, Y. Cui, M. Xu, L. Tu, Q. Chai, X. Zhou, Micro-lotus constructed by Fe-doped ZnO hierarchically porous nanosheets: preparation, characterization and gas sensing property, Sens. Actuators B 158 (2011) 9–16.

[23] L. Lin, T. Liu, Y. Zhang, X. Liang, R. Sun, W. Zeng, Z. Wang, Enhancing ethanol detection by heterostructural silver nanoparticles decorated polycrystalline zinc oxide nanosheets, Ceram. Int. 42 (2016) 3138–3144.

[24] Y. Xiao, L. Lu, A. Zhang, Y. Zhang, L. Sun, L. Huo, F. Li, Highly enhanced acetone sensing performances of porous and single crystalline ZnO nanosheets: high percentage of exposed (100) facets working together with surface modification with Pd nanoparticles, ACS Appl. Mater. Interfaces 4 (2012) 3797–3804.

[25] Y. Mun, S. Park, S. An, C. Lee, H. W. Kim, NO_2 gas sensing properties of Au-functionalized porous ZnO nanosheets enhanced by UV irradiation, Ceram. Int. 39 (2013) 8615–8622.

[26] D. Ju, H. Xu, Z. Qiu, J. Guo, J. Zhang, B. Cao, Highly sensitive and selective triethylamine-sensing properties of nanosheets directly grown on ceramic tube by forming NiO/ZnO PN heterojunction, Sens. Actuators B 200 (2014) 288–296.

[27] P. Wang, D. Wang, M. Zhang, Y. Zhu, Y. Xu, X. Ma, X. Wang, ZnO nanosheets/graphene oxide nanocomposites for highly effective acetone vapor detection, Sens. Actuators, B 230 (2016) 477–484.

[28] Z. Sun, T. Liao, Y. Dou, S. M. Hwang, M. S. Park, L. Jiang, J. H. Kim, S. X. Dou, Generalized self-assembly of scalable two-dimensional transition metal oxide nanosheets, Nat. Commun. 5 (2014) 3813.

[29] W. Guo, ZnO nanosheets assembled different hierarchical structures and their gas sensing properties, J. Mater. Sci.: Mater. Electron. 27 (2016) 7302–7310.

[30] Y. Yin, Y. Sun, M. Yu, X. Liu, B. Yang, D. Liu, S. Liu, W. Cao, M. N. R. Ashfold, Reagent concentration dependent variations in the stability and photoluminescence of silica-coated ZnO nanorods, Inorg. Chem. Front. 2 (2015) 28–34.

[31] J. Wang, X. Li, C. Teng, Y. Xia, J. Xu, D. Xie, L. Xiang, S. Komarneni, Ligand-directed rapid formation of ultralong ZnO nanowires by oriented attachment for UV photodetectors, J. Mater. Chem. C 4 (2016) 5755–5765.

[32] J. Li, H. Fan, X. Jia, Multilayered ZnO nanosheets with 3D porous architectures: synthesis and gas sensing application, J. Phys. Chem. C 114 (2010) 14684–14691.

[33] Y. Yin, Y. Sun, M. Yu, X. Liu, B. Yang, D. Liu, S. Liu, W. Cao, M. N. R. Ashfold, Arrays of nanorods composed of ZnO nanodots exhibiting enhanced UV emission and stability, Nanoscale 6 (2014) 10746–10751.

[34] U. Shaislamou, K. Krishnamoorthy, S. J. Kim, A. Abidov, B. Allabergenov, S. Kim, S. Choi, R. Suresh, W. M. Ahmed, H. J. Lee, Highly stable hierarchical *p*-CuO/ZnO nanorod/nanobranch photoelectrode for efficient solar energy conversion, Int. J. Hydrogen Energy 41 (2016) 2253–2262.

[35] Y.-P. Wu, W. Zhou, W.-W. Dong, J. Zhao, X.-Q. Qiao, D.-F. Hou, D.-S. Li, Q. Zhang, P Feng, Temperature-controlled synthesis of porous CuO particles with different morphologies for highly sensitive detection of trimethylamine, Cryst. Growth Des. 17 (2017) 2158−2165.

[36] Z. Wen, L. Zhu, Z. Zhang, Z. Ye, Fabrication of gas sensor based on mesoporous rhombus-shaped ZnOrod arrays, Sens. Actuators B 208 (2015) 112–121.

[37] N. T. P. Nhung, P. V. Tong, C. M. Hung, N. V. Duy, N. V. Chien, N. V. Vinh, N. T. Tuyen, N. D. Hoa, Nanoporous ZnO nanostructure synthesis by a facile method for superior sensitivity ethanol sensor applications, RSC Adv. 6 (2016) 64215–64218.

[38] J. Wang, C. Pei, L. Cheng, W. Wan, Q. Zhao, H. Yang, S. Liu, Responses of three-dimensional porous ZnO foam structures to the trace level of trimethylamine and ethanol, Sens. Actuators B 223 (2016) 650–657.

[39] L. Li, C. Zhang, R. Zhang, X. Gao, S. He, M. Liu, X. Li, W. Chen, 2D ultrathin Co_3O_4 nanosheet array deposited on 3D carbon foam for enhanced ethanol gas sensing application, Sens. Actuators B 244 (2017) 664–672.

[40] L. Li, M. Liu, S. He, W. Chen, Freestanding 3D mesoporous Co_3O_4@carbon foam nanostructures for ethanol gas sensing, Anal. Chem. 86 (2014) 7996–8002.

[41] L. Li, S. He, M. Liu, C. Zhang, W. Chen, Three-dimensional mesoporous graphene aerogel-supported SnO_2 nanocrystals for high-performance NO_2 gas sensing at Low temperature, Anal. Chem. 87 (2015) 1638−1645.

[42] N. S. Ramgir, P. K. Sharma, N. Datta, M. Kaur, A. K. Debnath, D. K. Aswal, S. K. Gupta, Room temperature H_2S sensor based on Au modified ZnO nanowires, Sens. Actuators B 186 (2013) 718–726.

[43] M. W. Roberts, The nature and reactivity of chemisorbed oxygen and oxide overlayers at metal surfaces as revealed by photoelectron spectroscopy, Stud. Surf. Sci. Catal. 48 (1989) 787–797.

[44] L. Li, C. Zhang, W, Chen, Fabrication of SnO_2–SnO nanocomposites with *p*–*n* heterojunctions for the low-temperature sensing of NO_2 gas, Nanoscale 7 (2015) 12133–12142.

Figure captions

Fig. 1. (a) SEM image, (b) TEM image, (c) AFM image and (d) XRD pattern of the pristine ZnO NSs. The height profile in the inset in (c) was measured by scanning along the red line, starting from the blue dot. The inset of (b) shows a HRTEM image of the sample.

Fig. 2. (a) TEM image, (b) HRTEM image, (c) XPS survey spectrum, and (d) high-resolution XPS spectrum of the Cu2p region for the '*12-min CuO-ZnO*' NS sample.

Fig. 3. Dynamic resistance of the pristine ZnO, '*2-min CuO-ZnO*', '*6-min CuO-ZnO*' and '*12-min CuO-ZnO*' NS samples exposed to 20 ppm ethanol at T_w of 320 ºC.

Fig. 4. Response and recovery curves of the pristine ZnO, '*2-min CuO-ZnO*', '*6-min CuO-ZnO*', and '*12-min CuO-ZnO*' NS samples upon exposure to 1–2000 ppm ethanol at T_w = 320 ºC. The inset shows the responses to 1–20 ppm ethanol on an expanded vertical scale.

Fig. 5. (a) Response of the '*6-min CuO-ZnO*' NS sample to repeat on–off exposures to 20 ppm of ethanol at T_w = 320 ºC, demonstrating the high repeatability of the sensing. (b) Response of the '*6-min CuO-ZnO*' NS sample to 200 ppm of ethanol and six other gases at T_w = 320 ºC.

Scheme 1. Schematic illustration of the ethanol sensing mechanisms of pristine ZnO NS samples (top) and CuO-ZnO NS samples (below).

Figure 1

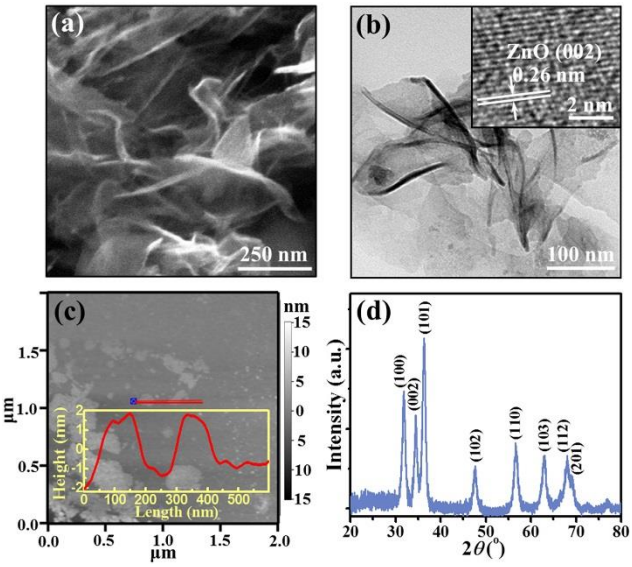
(a)
250 nm
(b)
ZnO (002)
0.26 nm
2 nm
100 nm
(c)
nm
15
10
5
0
5
10
15
1.5
1.0
0.5
0.0
μm
Height (nm)
Length (nm)
0 100 200 300 400 500
0.0 0.5 1.0 1.5 2.0
μm
(d)
Intensity (a.u.)
(100)
(002)
(101)
(102)
(110)
(103)
(112)
(201)
20 30 40 50 60 70 80
2θ(°)

Figure 2

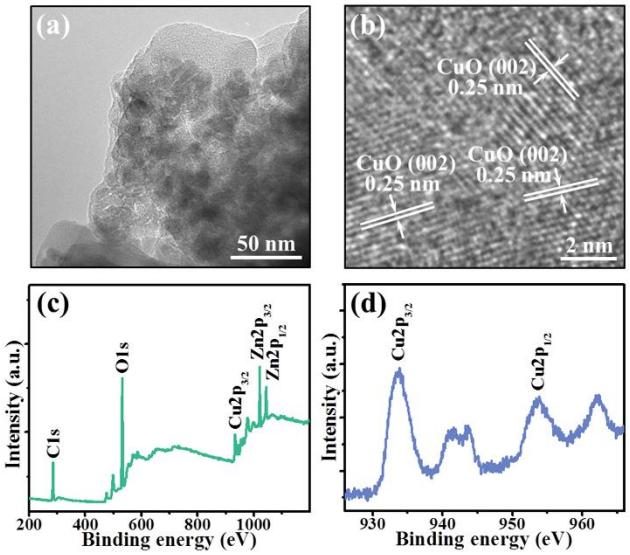
(a)
50 nm
(b)
CuO (002)
0.25 nm
CuO (002)
0.25 nm
CuO (002)
0.25 nm
2 nm
(c)
Intensity (a.u.)
C1s
O1s
Cu2p3/2
Zn2p3/2
Zn2p1/2
200
400
600
800
1000
Binding energy (eV)
(d)
Intensity (a.u.)
Cu2p3/2
Cu2p1/2
930
940
950
960
Binding energy (eV)

Figure 3

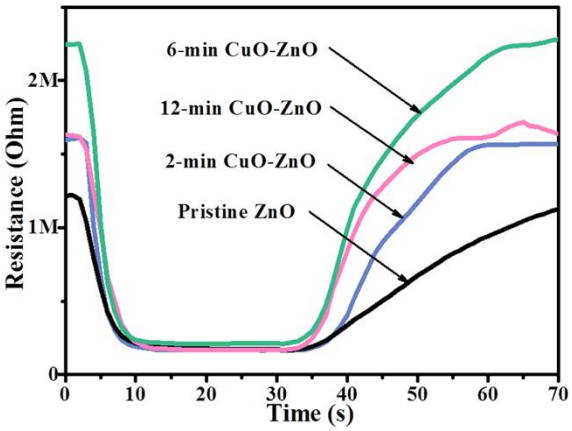
6-min CuO-ZnO
12-min CuO-ZnO
2-min CuO-ZnO
Pristine ZnO
Resistance (Ohm)
2M
1M
0
0
10
20
30
40
50
60
70
Time (s)

Figure 4

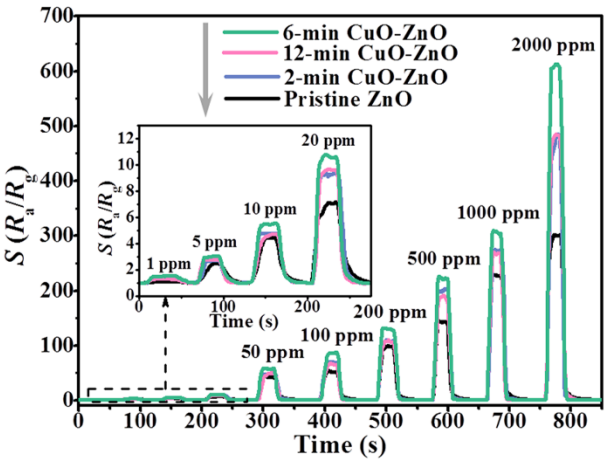
6-min CuO-ZnO
12-min CuO-ZnO
2-min CuO-ZnO
Pristine ZnO
2000 ppm
1000 ppm
500 ppm
200 ppm
100 ppm
50 ppm
20 ppm
10 ppm
5 ppm
1 ppm
S (Ra/Rg)
Time (s)

Figure 5

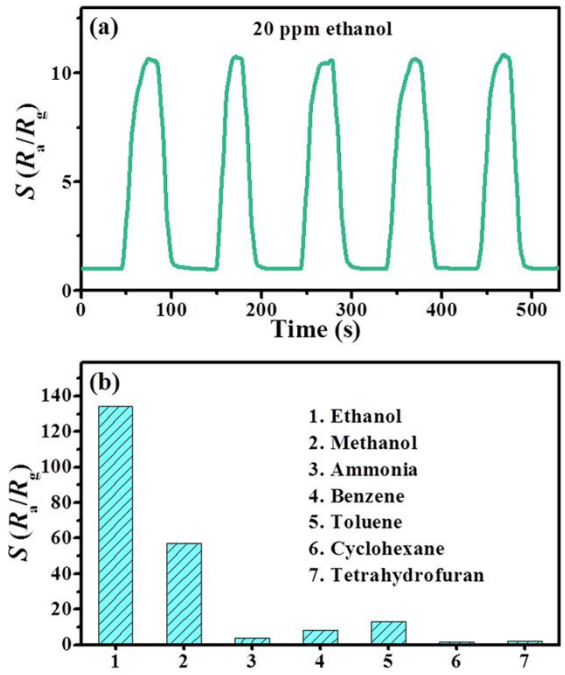
(a)
20 ppm ethanol
$S (R_a/R_g)$
Time (s)
(b)
1. Ethanol
2. Methanol
3. Ammonia
4. Benzene
5. Toluene
6. Cyclohexane
7. Tetrahydrofuran

Scheme 1

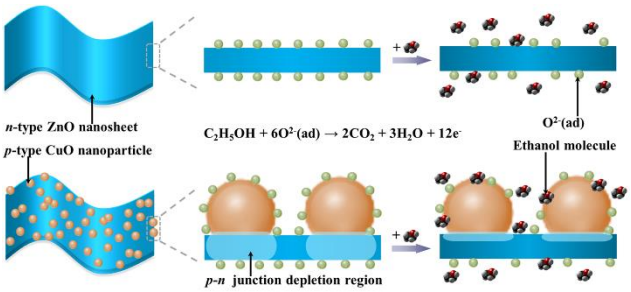
n-type ZnO nanosheet
p-type CuO nanoparticle
C2H5OH + 6O2-(ad) → 2CO2 + 3H2O + 12e-
O2-(ad)
Ethanol molecule
p-n junction depletion region